Statistics of whistler mode waves in the outer radiation belt: Cluster STAFF-SA measurements

Oleksiy Agapitov, Anton Artemyev, Vladimir Krasnoselskikh, Yuri V. Khotyaintsev, Didier Mourenas, Hugo Breuillard, Michael Balikhin, Guy Rolland

Statistics of whistler mode waves in the outer radiation belt: Cluster STAFF-SA measurements

Oleksiy Agapitov,[1,2,3] Anton Artemyev,[1,4] Vladimir Krasnoselskikh,[1]
Yuri V. Khotyaintsev,[5] Didier Mourenas,[6] Hugo Breuillard,[1]
Michael Balikhin,[7] and Guy Rolland[8]

[1] ELF/VLF waves play a crucial role in the dynamics of the radiation belts and are partly responsible for the main losses and the acceleration of energetic electrons. Modeling wave-particle interactions requires detailed information of wave amplitudes and wave normal distribution over L-shells and over magnetic latitudes for different geomagnetic activity conditions. We performed a statistical study of ELF/VLF emissions using wave measurements in the whistler frequency range for 10 years (2001–2010) aboard Cluster spacecraft. We utilized data from the STAFF-SA experiment, which spans the frequency range from 8 Hz to 4 kHz. We present distributions of wave magnetic and electric field amplitudes and wave normal directions as functions of magnetic latitude, magnetic local time, L-shell, and geomagnetic activity. We show that wave normals are directed approximately along the background magnetic field (with the mean value of θ— the angle between the wave normal and the background magnetic field, about $10°$–$15°$) in the vicinity of the geomagnetic equator. The distribution changes with magnetic latitude: Plasmaspheric hiss normal angles increase with latitude to quasi-perpendicular direction at $\sim 35°$–$40°$ where hiss can be reflected; lower band chorus are observed as two wave populations: One population of wave normals tends toward the resonance cone and at latitudes of around $35°$–$45°$ wave normals become nearly perpendicular to the magnetic field; the other part remains quasi-parallel at latitudes up to $30°$. The observed angular distribution is significantly different from Gaussian, and the width of the distribution increases with latitude. Due to the rapid increase of θ, the wave mode becomes quasi-electrostatic, and the corresponding electric field increases with latitude and has a maximum near $30°$. The magnetic field amplitude of the chorus in the day sector has a minimum at the magnetic equator but increases rapidly with latitude with a local maximum near $12°$–$15°$. The wave magnetic field maximum is observed in the night sector at $L > 7$ during low geomagnetic activity (at $L \sim 5$ for $K_p > 3$). Our results confirm the strong dependence of wave amplitude on geomagnetic activity found in earlier studies.

1. Introduction

[2] The majority of the models describing the formation and dynamics of the radiation belts treat wave-particle interactions within the framework of the quasi-linear approximation and should take into account the dependence of the wave parameter distribution on the L-shell (L), magnetic latitude (λ), and magnetic local time (MLT). The particle diffusion is supposed to be slow compared with the particle bounce time between the mirror points along the magnetic field line. Thus, the diffusion coefficients are evaluated using averaging over fast timescales, namely, the gyroperiod and the bounce time between the mirror points. The knowledge

Corresponding author: O. Agapitov, LPCE/CNRS, University of Orleans, Orleans, France; LE STUDIUM, Loire Valley Institute for Advanced Studies, University of Orleans and University of Tour, LPC2E/CNRS-University of Orleans, 3A avenu de la Recherche Scientifique, Orleans CEDEX 2, 45171, France; Astronomy and Space Physics Department, National Taras Shevchenko University of Kiev, Kiev, Ukraine. (agapit@univ.kiev.ua)

[1]LPC2E/CNRS, University of Orleans, Orleans, France.
[2]LE STUDIUM, Loire Valley Institute for Advanced Studies, University of Orleans and University of Tour, Orleans, France.
[3]Astronomy and Space Physics Department, National Taras Shevchenko University of Kiev, Kiev, Ukraine.
[4]Space Research Institute, Moscow, Russia.
[5]Swedish Institute of Space Physics, Uppsala, Sweden.
[6]CEA, DAM, DIF, F-91297, Arpajon, France.
[7]Department of Automatic Control and Systems Engineering, University of Sheffield, Sheffield, South Yorkshire, UK.
[8]CNES, Toulouse, France.

of the energy density of the waves in resonance with particles along a particular L-shell for different λ is required for the calculation of the electron diffusion rates [*Kennel and Petschek*, 1966; *Lyons and Thorne*, 1973; *Lyons*, 1974a, 1974b]. Now several numerical and semi-analytical models of diffusion coefficients have been developed [see *Glauert and Horne*, 2005; *Summers et al.*, 2007, and reference therein]. In these models, mean value of θ (the angle between the wave normal and the magnetic field) is assumed to be equal to zero. Another assumption is that the wave power along each L-shell is constant [*Glauert and Horne*, 2005; *Summers et al.*, 2007] or approximated by a simple stepwise function [*Ni et al.*, 2011]. These simplifications are used due to the lack of observational data of these distributions. The results of diffusion rate estimations are quite sensitive to the characteristics of the assumed distribution [*Glauert and Horne*, 2005; *Shprits and Ni*, 2009]. The previously calculated rates of relativistic electron acceleration and scattering by chorus waves have been based on time-averaged spectral densities, which, as it was pointed out by *Cully et al.* [2008] and *Agapitov et al.* [2011b], may not be fully representative of realistic conditions. Wave amplitudes also have a significant probability in the tail of the probability distribution function [*Cully et al.*, 2008; *Agapitov et al.*, 2011b; *Bunch et al.*, 2012], which makes the use of averaged values potentially misleading over the short term. In order to improve the description of wave-particle resonant interactions, one should take into account the inhomogeneity of the distribution of the wave electromagnetic field along the magnetic flux tube and describe the effects of oblique wave propagation with respect to the background magnetic field.

[3] The distribution of the chorus wave normal angles has been a subject of interest during the past few decades. Nevertheless, it has mainly been studied in the vicinity of the equator [*Hayakawa et al.*, 1984; *Lauben et al.*, 2002; *Goldstein and Tsurutani*, 1984; *Burton and Holzer*, 1974; *Agapitov et al.*, 2010; *Li et al.*, 2011; *Agapitov et al.*, 2011a]. Based on previous measurements, values of θ have generally been estimated as less than $30°$. Several cases of oblique chorus and hiss wave propagation were, however, found in Cluster measurements in the generation region [*Santolík et al.*, 2009; *Chum et al.*, 2009], showing that the assumption of a parallel propagation may be insufficient even near the equator. The systematic behavior of θ was studied by *Burton and Holzer* [1974], *Hayakawa et al.* [1984], *Muto et al.* [1987], *Haque et al.* [2010], and *Agapitov et al.* [2011b]. Using 18 passes of the OGO5 spacecraft, *Burton and Holzer* [1974] found that θ was less than $30°$ for $|\lambda| < 40°$ (80% of the events) for the lower band chorus and that θ extended to $85°$ for $|\lambda| > 40°$ with a spreading of the distribution of angles. *Hayakawa et al.* [1984] and *Muto et al.* [1987] showed that the upper band chorus can propagate very close to the local resonant cone θ_{res}, while the lower band chorus has usually a relatively small θ of about $5°$–$40°$. A similar behavior for the upper band chorus waves was found by *Haque et al.* [2010] on the basis of Polar measurements, while the direction of propagation for the lower band chorus waves was also found to be close to the background magnetic field. The statistics of the whistler waves normal directions was presented by *Agapitov et al.* [2011b, 2012] for $|\lambda| < 30°$ from 10 years of Cluster measurements.

It was shown that wave normals of the chorus and hiss waves move away from the direction of the background magnetic field when λ increases, starting from the equator with a mean value of $\theta \sim 10°$–$15°$. These results were confirmed by ray-tracing numerical calculation of the wave normal distribution by *Breuillard et al.* [2012]. Similar results for the wave normal distribution near the geomagnetic equator were presented by *Goldstein and Tsurutani* [1984] and *Li et al.* [2011] for the chorus waves detected by the OGO-5 and Thermal Emission Imaging System (THEMIS) spacecraft, respectively. For the plasmaspheric hiss, a similar behavior was found by *Bortnik et al.* [2011] by means of ray tracing. Numerical calculation of the diffusion coefficients presented by *Artemyev et al.* [2012a] taking into account the θ dependence on λ showed significant effects for electron pitch angle diffusion rates in the radiation belts. It results in an increase of the role of higher order cyclotron harmonic resonances and leads to a significant growth of electron pitch angle diffusion rates, especially for low equatorial electron pitch angles [*Shprits and Ni*, 2009; *Artemyev et al.*, 2012a]. Intense oblique chorus waves can therefore lead to an important decrease of electron lifetime in the outer radiation belt [*Mourenas et al.*, 2012a].

[4] Despite the large number of the above-reported studies, a general consensus has not yet been reached regarding the chorus wave normal angle distribution. Here we investigate how the wave amplitudes, the wave normals, and the field-aligned Poynting flux depends upon λ, the L-shell, and geomagnetic activity (K_p -index) in a wide region around the geomagnetic equator ($|\lambda| < 45°$), at radial distances from 2 to 7 R_E as covered by Cluster from 2001 to 2010. The present paper first rectifies some inaccuracies in *Agapitov et al.* [2011b], which were caused by erroneous referential frame specifications in CLUSTER's CAA (Cluster Active Archive) data set (now assessed and fixed) [*Agapitov et al.*, 2012]. Furthermore, this paper extends the studies by *Agapitov et al.* [2011b] by taking into account a broader range of latitudes and considering statistics of both the wave magnetic and electric field amplitudes. Special attention is paid to the behavior of wave normals (from the spectral matrices and from wave electric and magnetic field power ratio), their possible approach to the resonance cone and the progressive transformation of chorus from a quasi-electromagnetic mode to a quasi-electrostatic mode. Also, the statistics of the wave normal angles and wave magnetic and electric field amplitudes are presented in the form of probability density functions (PDF).

2. Data Set and Analysis Technique

[5] For this work, we made use of the data set of ELF/VLF waves observed by Cluster between February 2001 and December 2010 in the radiation belts (i.e., confined for the $|\lambda| < 45°$ and $2 \leq L \leq 7$). This region is thought to be of primary importance for the generation of chorus waves. The Cluster data set contains a sufficient number of measurement points for performing a statistical study for the considered range of magnetic local times (MLT) and L-shells, as illustrated in Figure 1. Our analysis is based on the data from the Spatio-Temporal Analysis of Field Fluctuations - Spectrum Analyzer (STAFF-SA) experiment [*Cornilleau-Wehrlin et al.*, 2003], which provides the
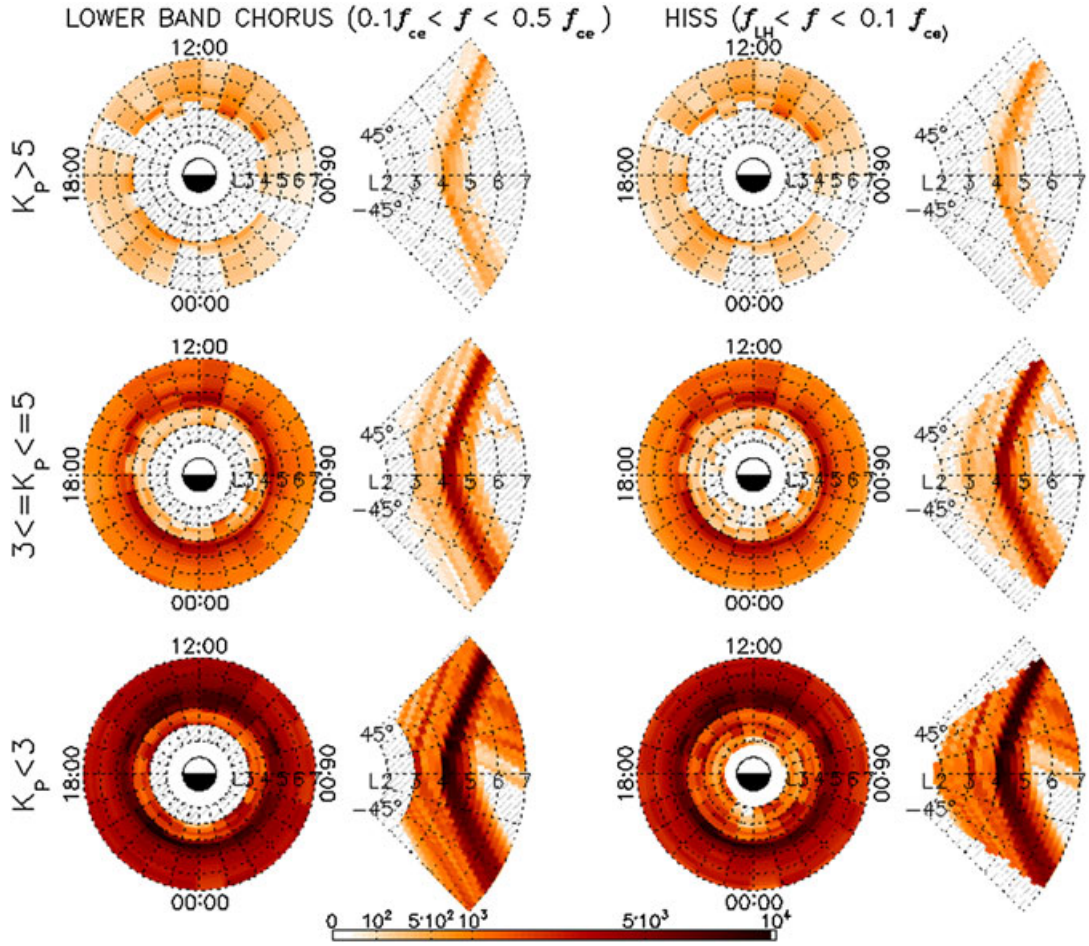
Figure 1. Data coverage for the CLUSTER STAFF-SA measurements during 2001–2010 (left panels) for the LB chorus frequency range ($0.1f_{ce} < f < 0.5f_{ce}$) and (right panels) for the hiss frequency range ($f_{LH} < f < 0.1f_{ce}$) in dependence on L-shell, (bottom panels) λ and MLT for periods of low ($K_p < 3$), (top panels) intermediate ($3 \le K_p \le 5$) and high geomagnetic activity ($K_p > 5$).

complete spectral matrix (the real and the imaginary part) of the three magnetic components as measured by the STAFF search coil magnetometer and the Electric Fields and Waves instrument measurements of two components of wave electric field [*Gustafsson et al.*, 2001]. Our survey includes STAFF-SA data from the Cluster 4 spacecraft (Samba) in order to avoid different statistical contributions due to different cross-spacecraft distances during the processing period. We use Spectral Matrices and Power Spectral Density data provided by Cluster Active Archive in SR2 (Spin Reference) frame. The analyzed wave frequency range included electron whistler waves from the lower-hybrid frequency f_{LH} up to the electron cyclotron frequency f_{ce}. This range is known to be dominated by the plasmaspheric hiss (mainly from f_{LH} to approximately $0.1 f_{ce}$) [*Thorne et al.*, 1973; *Meredith et al.*, 2006], by the lower band (LB) chorus ($0.1f_{ce} < f < 0.5f_{ce}$) and by the upper band (UB) chorus waves ($0.5f_{ce} < f < 1.0f_{ce}$). Hiss waves can be observed above $0.1 f_{ce}$, but their intensity rapidly falls above 1 kHz [*Meredith et al.*, 2004]. In this paper, we consider plasmaspheric hiss as observed in the plasmasphere whistler waves with frequency below $0.1 f_{ce}$ on the equator (but below 2000 Hz) and above the local f_{LH} (that determines the L-shell range to be from 2 to the plasmapause). Plasmapause position with dependence

on MLT is estimated from the model by *Doe et al.* [1992]. The spectral matrix was computed onboard for 27 frequency channels that were logarithmically spaced between 8.8 Hz and 3.56 kHz (central frequencies). The availability of the STAFF-SA frequency channels for chorus (LB and UB) and hiss is the following: For the LB chorus, the full range of L-shells and magnetic latitudes is available (for $L > 4$ coverage by five to seven channels). Thus, the LB chorus was studied mainly out of the plasmasphere. The behavior of the UB chorus can be studied only for $L > 6$, where Cluster has very poor coverage near the equator (see Figure 1), leading us to exclude the UB chorus from the statistics [*Agapitov et al.*, 2012]. Additionally, the UB chorus is substantially less intense than the LB chorus [*Meredith et al.*, 2001; *Haque et al.*, 2010]. As concerns hiss, the range of L-shells is available from 2 to the plasmapause covered by two ($L = 2$) or more (four at $L = 3$ and eight at $L = 4$) frequency channels for $|\lambda| < 30°$. The sensitivity of the STAFF search coil magnetometers is $3 \cdot 10^{-3}$ nT Hz$^{-1/2}$ at 1 Hz, and about $3 \cdot 10^{-5}$ nT Hz$^{-1/2}$ between 100 Hz and 4 kHz [*Cornilleau-Wehrlin et al.*, 2003]. We excluded measurements with amplitudes below the double of the STAFF-SA sensitivity level from wave normal angle processing but took them into account for wave amplitude analysis.

[6] For data analysis, we used a technique of wave normal vector $\vec{k}$ evaluation under the assumption of single planar wave propagation, as suggested by *Means* [1972]. It involves the computation of a spectral matrix that consists of the power and the cross-power spectra using three magnetic components. The Means wave normal evaluation method was applied by *Cornilleau-Wehrlin et al.* [1997] to recover the direction of the injected signal wave normal, and the results have been compared with the results of two other methods (minimum variance analysis of magnetic field perturbations—MVAB and wave distribution function—WDF) which can be used when the waves are assumed to be single and planar. Several independent realizations of noisy samples have been used to calculate the spectral matrices. At high signal-to-noise ratios, it was observed that the wave normal direction is well recovered by all three methods, with errors always smaller than 10° for signal-to-noise ratios greater than one. For the observed chorus waves, this ratio was mostly greater than 1.5 and was even about 2 in general. Here we present results obtained by the Means method but verified by the MVAB technique (applicability of the single plane wave approximation and signal-to-noise ratio were controlled by real part of spectral matrix eigen number values ratios). The method has an inherent 180° ambiguity in the wave normal direction that can be resolved if the Poynting vector $\vec{S}$ is known. Since the wave normal must have a component in the direction of energy flow, the scalar product $(\vec{S} \cdot \vec{k})$ should indeed be positive.

[7] Chorus waves that are generated at different locations propagate along different trajectories and can be detected simultaneously at the same point. Thus, it is necessary to know if more than one wave is present in the processed data. To control the applicability of the single plane wave approximation, we investigate the ratios of maximal-intermediate (λ_1/λ_2) and intermediate-minimal (λ_2/λ_3) eigen values of the real part of spectral matrices. Considering single plane wave propagation and taking into account the circular right-hand polarization of whistler waves, led us to include only $\lambda_1/\lambda_2 < 2$ data into wave normal statistics. We found that the approximation of single wave propagation was not valid only in a very small number of cases (less than 2%), which have a negligible effect on the statistical results. The signal-to-noise ratio for chorus and hiss was controlled by λ_2/λ_3 ratio: Data with $\lambda_2/\lambda_3 < 2$ was eliminated from the analysis. Signal-to-noise ratio limitation eliminates about 40% of data from wave normal statistics.

[8] The spectral matrices registered by the STAFF-SA allowed to evaluate the Poynting flux components along the spacecraft spin axis and to reconstruct the component along the background magnetic field $\vec{S} = (1/2)\,\mathrm{Re}\,[\vec{E}_w(f) \times \vec{B}_w^{\,*}(f)]$. Here, * indicates the complex conjugate, Re represents the real part, $\vec{E}_w(f)$ and $\vec{B}_w(f)$ are the Fourier transforms of the electric and the magnetic field waveforms (they are obtained from the spectral matrix components for 27 frequencies). The wave-normal angles were obtained by applying the above-described procedure.

[9] Figure 2 shows (a) the magnetic field spectral power, (b) the wave normal angle θ, (c) refractive index n, (d) wave electric field absolute value (the third component was restored by use of the approximation of $\vec{E}_w \cdot \vec{B}_w = 0$), and (e) ratio ($c|B_w|/|E_w|$) during the crossing of the geomagnetic
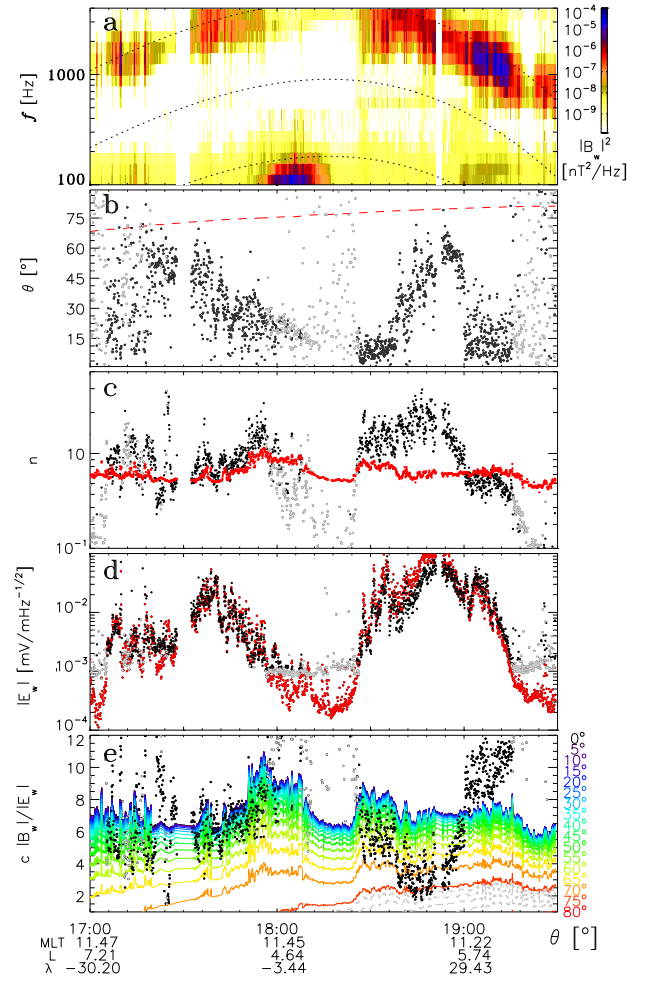

Figure 2. Cluster 4 spacecraft crossing of the geomagnetic equator on 16 September 2003: (a) wave magnetic field spectral power. Equatorial values of f_{LH}, 0.1 f_{ce}, and 0.5 f_{ce} are shown by dashed lines; (b) estimation of θ from C4 STAFF-SA spectral matrices for STAFF-SA channel with central frequency equal to 2244.9 Hz (here and in the following panels, values estimated for spectral power amplitudes below the STAFF-SA noise level are indicated by grey color). θ_{res} is indicated by red dashed line; (c) refractive index $\widetilde{n}$, evaluated from $|E_w|/|B_w|$ ratio (black and grey circles). The estimation of $n_\parallel$ obtained with approximation $\vec{k} \| \vec{B}_0$ is indicated by red line; (d) wave electric field absolute value from STAFF-SA with the third component restored from $\vec{B}_w \vec{E}_w = 0$ (red circles). The value of E_w re-calculated from equation (2) is shown by black (and grey) circles; (e) ratio $c|B_w|/|E_w|$ (black and grey circles). The estimations of this ratio obtained from background magnetic field and plasma parameters (equation (2)) are shown for a wide range of θ values from 0° to 80°, indicated by colors from black to red.

equator by the Cluster C4 spacecraft on 16 September 2003. An increase of θ with $|\lambda|$ is observed in Figure 2b (here θ was estimated by use of the STAFF-SA spectral matrices). θ approaches the resonance cone angle (shown by the dashed red line) at $|\lambda| \simeq 25$–30° and decreases above. All results

obtained for magnetic field measurements here and in the other panels of Figure 2 for magnetic field spectral power below the STAFF-SA noise level are indicated by grey color. n is estimated from the cold-plasma dispersion relation for the whistler mode:

$$n^2 = \frac{RL\sin^2\theta + PS(1+\cos^2\theta)}{2\left(S\sin^2\theta + P\cos^2\theta\right)}$$
$$-\frac{\sqrt{\left(RL\sin^2\theta + PS(1+\cos^2\theta)\right)^2 - 4PRL\left(S\sin^2\theta + P\cos^2\theta\right)}}{2\left(S\sin^2\theta + P\cos^2\theta\right)},$$

$$(1)$$

where R, L, P, and S are the Stix parameters [*Stix*, 1962]:

$$R = 1 - \left(\frac{f_{pe}}{f_{ce}}\right)^2 \left(\frac{f_{ce}}{f}\right)\left[\left(\frac{f_{ce}}{f}\right) - 1\right]^{-1},$$

$$L = 1 - \left(\frac{f_{pe}}{f_{ce}}\right)^2 \left(\frac{f_{ce}}{f}\right)\left[\left(\frac{f_{ce}}{f}\right) + 1\right]^{-1},$$

and $S = (R+L)/2, D = (R-L)/2, P = 1 - \left(\frac{f_{pe}}{f}\right)^2, f_{pe}$ is the local plasma frequency. The re-calculated by use equation (1) values of $n_{\parallel}$ in the approximation of parallel wave propagation (from magnetic field Flux Gate Magnetometer (FGM) magnetic field measurements [*Balogh et al.*, 2001] and electron density Electric Filed and Wave instrument (EFW) evaluations [*Khotyaintsev et al.*, 2010]) are shown by red circles in Figure 2c. This indicates the lower limit of n. The estimated values of n from STAFF-SA wave magnetic and electric intensity ratio—$\widetilde{n}$ are shown by black circles. $\widetilde{n}$ increases with θ from ~ 7 on the equator to several tens for $\theta \sim \theta_{res}$. The disagreement of $n_{\parallel}$ and $\widetilde{n}$ indicates obliqueness of wave normal direction in relation to the background magnetic field.

[10] The wave electric field spectral power $|E_w|$ can be re-calculated from Faraday's law by use of $|B_w|$ and polarization properties:

$$B_w^2 = E_w^2 \frac{n^2}{c^2}\sin^2\beta, \qquad (2)$$

where β is the angle between $\vec{E}_w$ and $\vec{k}$ determined from the dispersion matrix and Maxwell equations as [*Ni et al.*, 2011]:

$$\cos\beta = \frac{\sin\theta(n^2 - P)}{\sqrt{(n^2\sin^2\theta - P)^2 + \frac{D^2(n^2\sin^2\theta - P)^2}{(n^2 - S)^2} + n^4\sin^2\theta\cos^2\theta}}. \quad (3)$$

[11] A good agreement is obtained between $|E_w|$ measured by STAFF-SA (shown by red circles in Figure 2d) and re-calculated from relation equation (2) (shown by black and grey circles in Figure 2d). The independent estimation of θ can be provided from ratio $|B_w|/|E_w|$ by use of equations (2) and (1). The ratio $(c|B_w|/|E_w|)$ from STAFF-SA wave electric and magnetic field measurements is shown in Figure 2e by black circles. Re-calculated from background conditions values of $(c|B_w|/|E_w|)$ for the full range of θ are shown in Figure 2e with solid lines (the values of θ are indicated by color). The good agreement between Figures 2b and 2e shows applicability of used approximations and potential perspectives to process normal angle from magnetic and electric field wave power measurements.

3. Statistical Characteristics of ELF/VLF Waves in the Inner Magnetosphere

[12] Here we present the statistical results for wave magnetic and electric field captured by STAFF-SA during 2001–2010 in the form of an averaged wave intensity and the wave normal direction. We consider the dependencies on the following parameters: (1) the location of the wave detection (the L-shell, the MLT, and λ), (2) the wave characteristics (the wave frequencies normalized to the equatorial values of f_{ce} (calculated from the dipolar approximation), the magnitude of the wave magnetic and the electric fields, and the wave vector direction relative to the background magnetic field), and (3) the geomagnetic activity conditions as characterized by the K_p-index. We process intermediate ($3 \leq K_p \leq 5$) and high geomagnetic activity ($K_p > 5$) time intervals together, because of poor statistics for high geomagnetic activity periods. The statistical properties for the chorus wave distribution are rather similar for these two geomagnetic activity levels [*Agapitov et al.*, 2011b; *Pokhotelov et al.*, 2008].

3.1. Statistical Characteristics of ELF/VLF Waves Magnetic and Electric Field Amplitudes in the Inner Magnetosphere

[13] Using wave magnetic and electric field data from Cluster STAFF-SA, a database has been built to study the spatial distribution of whistler mode wave power. The data were binned in steps of 0.1 L, 1 h of MLT, 1° of λ, and 1° of θ. The background magnetic field was obtained from Cluster FGM measurements [*Balogh et al.*, 2001]; geomagnetic activity indices and interplanetary magnetic field data were used as extracted from NASA/Goddard Space Flight Center's OMNI (Operating Missions as a Node on the Internet) data set through OMNIWeb [*King and Papitashvili*, 2005]. Magnetic and electric field amplitudes were binned on a logarithmic scale in steps of $0.1 \log|nT \cdot Hz^{-\frac{1}{2}}|$ and $0.1 \log|mV/m \cdot Hz^{-\frac{1}{2}}|$, respectively. Usually, the observed wave amplitudes have distributions which are significantly non-Gaussian. Here we present averaged magnetic field intensity distribution and the PDFs for magnetic and electric field amplitude dependence on λ, which allow one to calculate the PDF for particle diffusion coefficients [*Artemyev et al.*, 2012b]. The averaged magnetic field intensity is shown in Figure 3 and Figure 5 for chorus and plasmaspheric hiss, respectively. *Tsurutani and Smith* [1977] and *Meredith et al.* [2001] showed that chorus can be divided into two categories depending on λ: equatorial $|\lambda| < 15°$ and midlatitude chorus $15° < |\lambda| < 45°$. The distribution properties of these two populations are different. We use here such a separation for MLT/L-shell diagrams for chorus and hiss.

[14] The equatorial LB chorus $|B_w|$ and occurrence rate are shown in Figures 3a and 3b for $K_p \leq 3$ and in Figures 3c and 3d for $K_p > 3$ in L-shell/MLT frame. Occurrence rate is calculated as the ratio of number of measurements of waves with $|B_w| > 1$ pT on the total number of measurements in each bin. Chorus mainly are observed outside the plasmasphere (modeled plasmapause position is shown by solid line). During quiet conditions, $|B_w|$ are less than 20 pT over the entire region with the maximum in the dawn and prenoon sector at $6 < L < 8$. Intense waves are observed also on $L > 9$, from 10:00 to 14:00 MLT, possibly connected
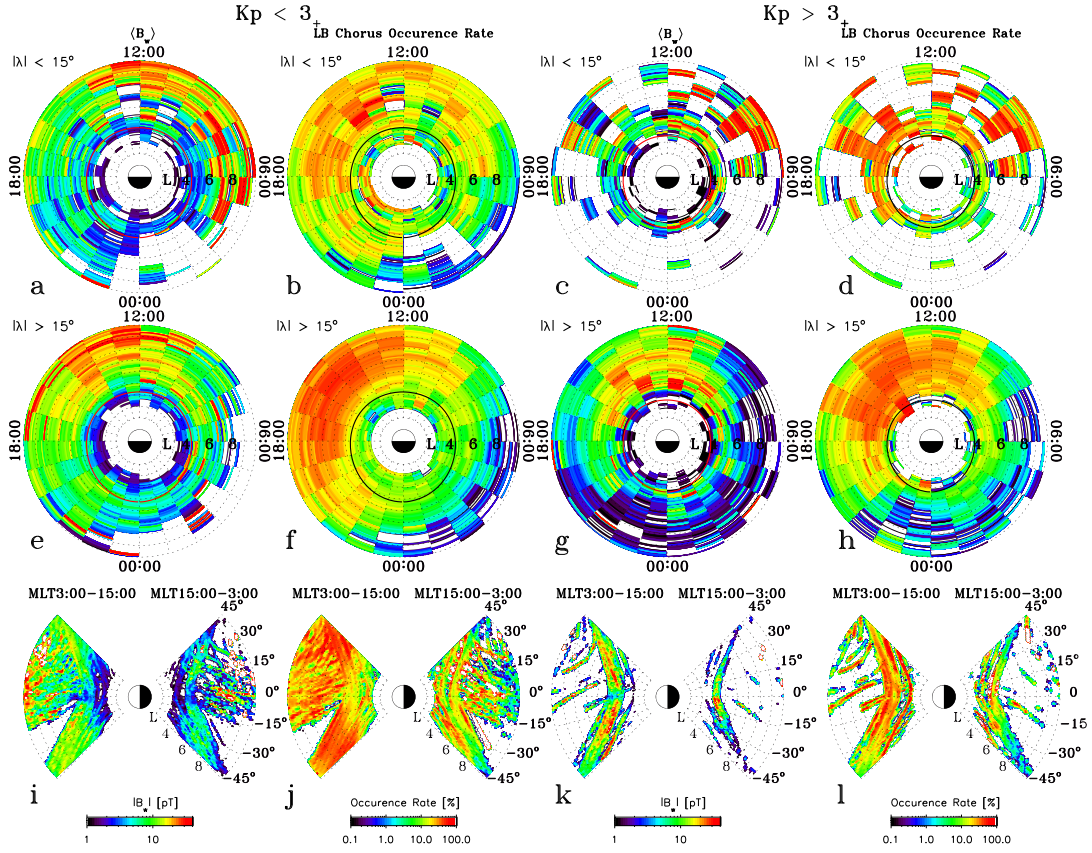
Figure 3. (a) Equatorial chorus averaged wave intensity and (b) occurrence rate shown in *L*-shell/MLT frame for quiet geomagnetic conditions ($K_p \leq 3$). (c and d) Distributions of averaged intensity and occurrence rate for disturbed conditions ($K_p > 3$) are shown, respectively. Distributions for midlatitude chorus are shown in Figures 3e and 3f $K_p \leq 3$ and 3g and h $K_p > 3$ in the same format. (i) Chorus averaged wave intensity and (j) occurrence rate are shown in *L*-shell/λ frame for $K_p \leq 3$, Figures 3k and 3l, respectively, show distributions for $K_p > 3$.

to secondary chorus sources in the dayside magnetic field pockets [*Tsurutani and Smith*, 1977]. Occurrence rate is quite close to the observed by THEMIS spacecraft in the equatorial region [*Cully et al.*, 2008; *Li et al.*, 2011; *Meredith et al.*, 2012]. Wave intensity distribution is consistent with observed by other spacecraft compared and brought together with DE1, CRRES, TC1, and THEMIS LB chorus intensity measurements to the common database in *Meredith et al.* [2012]. The midlatitude LB chorus intensity and occurrence rate are shown in Figures 3e and 3f. The spatial dependence of the distribution is different from the equatorial LB chorus. The amplitudes are close, but the peak of intensity is shifted to the afternoon sector 12:00–15:00 MLT and $6 < L < 10$ with larger occurrence rate ($> 60\%$).

[15] The LB chorus statistics for $K_p > 3$ is poor (especially in the vicinity of the equator): It can be seen that amplitudes and occurrence rate of equatorial LB chorus are generally larger than during low geomagnetic activity (up to 50 pT and more than 60%). Waves with amplitudes greater than 1 pT are observed closer to the Earth near the position of the plasmapause. At $4 < L < 5$, Cluster STAFF-SA measurement coverage is good, and for this range of *L*-shell, the distribution of $|B_w|$ dependence on MLT has maximal values from 02:00 to 14:00 MLT. The most intense chorus are

observed in the outer magnetosphere ($L > 6$) in the pre-noon sector (here it can be caused by measurement gap especially for $L > 5$). The Cluster STAFF-SA measurement coverage for $|\lambda| > 15°$ is sufficient for statistical analysis. Midlatitude LB chorus during high geomagnetic activity has maximum in intensity at $L \sim 5$–6, 10:00–14:00 MLT. The intensity and occurrence rate peaks are closer to the Earth than they are during quiet geomagnetic activity.

[16] The dependence of chorus magnetic field averaged intensity and chorus occurrence rate in *L*-shell/λ frame is presented in Figures 3i– 3l. The magnetic field amplitude minimum is obtained in the day and night sectors at *L*-shells from 4 to 6 during the quiet geomagnetic conditions ($K_p \leq 3$). Magnetic field amplitude maximum is observed at $\lambda \sim 10°$–20° and above 25°–30° $|B_w|$ decreases. More details can be seen in Figure 4 where the dependencies of LB chorus magnetic and electric field amplitude distribution on λ for $4 < L < 6$ are shown. At $L > 6$ in the night equatorial region $|\lambda| < 10°$, the amplitude maximum is observed (Figure 3i) presumably due to direct particle injection from the plasma sheet ($K_p \leq 3$). This $|B_w|$ maximum shifts toward the Earth during high geomagnetic activity and is observed at $L \sim 4$–5 and $|\lambda| < 15°$. LB chorus occurrence rate is high for all λ in the day sector for $5 < L < 10$ during low
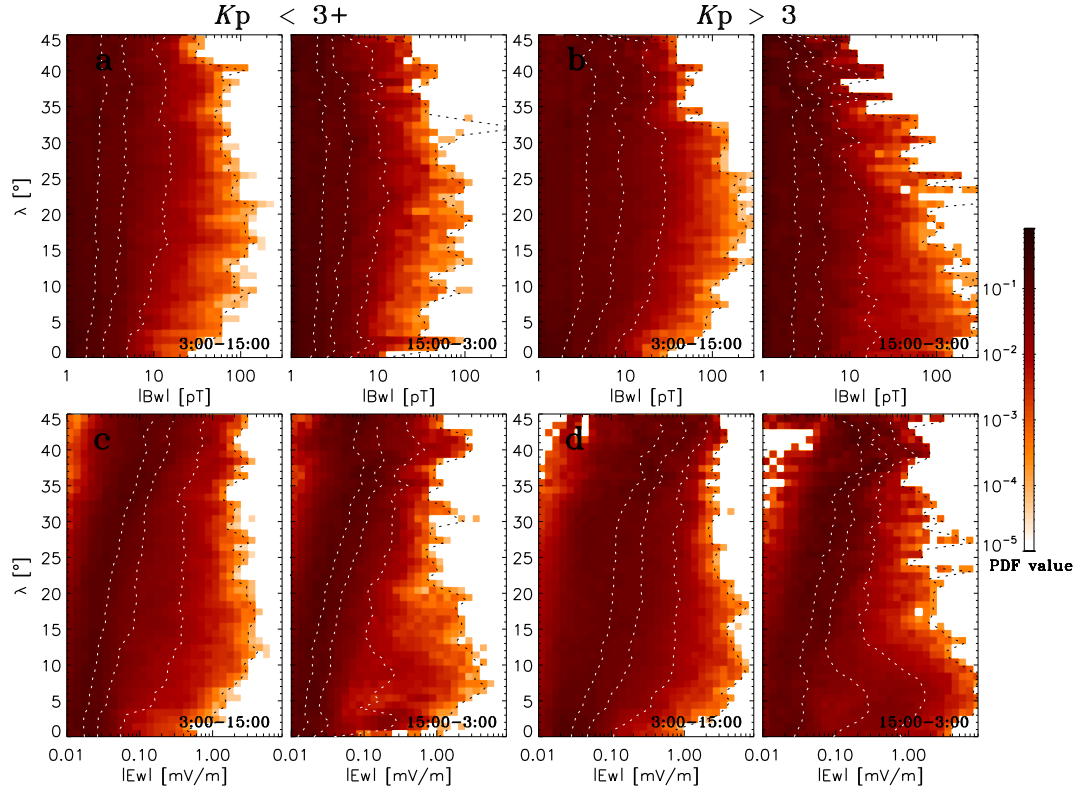
Figure 4. Chorus wave amplitudes of (top) wave magnetic and (bottom) electric field perturbations for different geomagnetic activity ($4 < L < 5.5$). The probability density function is shown for $|\lambda| < 45°$. The probability cumulative function levels 0.5, 0.75, 0.95, and 0.999 are indicated with dashed lines.

geomagnetic activity and for $4 < L < 8$ for $K_p > 3$. In the night sector, occurrence rate generally is lower and has maximal values $\sim 60\%$ at $4 < L < 8$ for $K_p < 3$ and $4 < L < 6$ for $K_p > 3$. Obtained dependencies on L-shell $- \lambda$ are well consistent with localization of high amplitude chorus waves (wave magnetic amplitude minimum on equator in the day sector and maximum in the night sector for high geomagnetic activity) obtained from CRRES measurements in the day/night sectors $3 < L < 7$ [*Meredith et al.*, 2004, 2012; *Horne et al.*, 2005].

[17] Figure 4 shows the PDFs of the LB chorus magnetic (Figures 4a and 4b) and electric field (Figures 4c and 4d) wave amplitudes for each λ. Amplitude (0.5, 0.75, 0.95, and 0.999) levels for the probability cumulative functions (PCF) are indicated with dashed lines. Thus, the amplitude range from 0.75 to 0.999 of PCF includes 25 percents of all events with maximal amplitudes. The averaged wave intensity level approximately corresponds to 0.75 level of PDF. The high amplitude chorus distribution has a peak around $|\lambda| \approx 20°$. During periods of low geomagnetic activity, the highest wave amplitudes vary from 10 pT at the equator to 90 pT. The 0.5 level does not show clear dependence on λ, just a decrease for $|\lambda| > 35°$. Similar dependencies are observed in the day sector during high geomagnetic activity periods (Figures 4b and 3), but the amplitudes are higher, and the increase with λ is faster: from 20 pT at the equator to more than 100 pT for $|\lambda| \approx 30°$. In the night MLT sector, chorus wave amplitudes peak around 100 pT for $|\lambda| < 10°$ and then decrease. Similar results were obtained by *Horne*

et al. [2005] from CRRES data. In contrast to chorus waves, hiss waves demonstrate rather constant amplitudes for all λ (Figure 5).

[18] The plasmaspheric hiss $|B_w|$ and occurrence rate are shown in Figures 5a and 5b for $K_p \leq 3$ and in Figures 5c and 5d for $K_p > 3$ in L-shell/MLT frame. High amplitude hiss waves are principally observed at 10:00–22:00 MLT with intensity maximum about 10 pT at $4 < L < 5$ during quiet geomagnetic activity and up to 15 pT at $3 < L < 4$ during high. Maximum of the occurrence rate MLT is shifted during high geomagnetic activity periods from 13:00–24:00 to 10:00–20:00 MLT. The equatorial and midlatitude distributions do not differ significantly (as well as the occurrence rate), but amplitudes of midlatitude plasmaspheric hiss are generally smaller than equatorial values. The intense waves observed at MLT from 2:00 to 6:00 (Figure 5e) can be LB chorus waves propagating near the plasmapause.

[19] The plasmaspheric hiss intensity and occurrence rate distribution in L-shell/λ frame distribution show rather constant wave amplitude values for different λ (Figures 5i–5l) and intensity peak at $3 < L < 5$ with high occurrence rate during low and high geomagnetic activity ($> 50\%$).

[20] The obtained distributions for chorus and hiss are close to the distributions of averaged wave power presented by *Pokhotelov et al.* [2008] and occurrence rate presented by *Agapitov et al.* [2011b]. In this work, we extended studies of Cluster STAFF-SA wave statistics [*Pokhotelov et al.*, 2008; *Agapitov et al.*, 2011b; *Meredith et al.*, [*Meredith et al.*, 2012]] by using Cluster data collected from 2006 to 2010
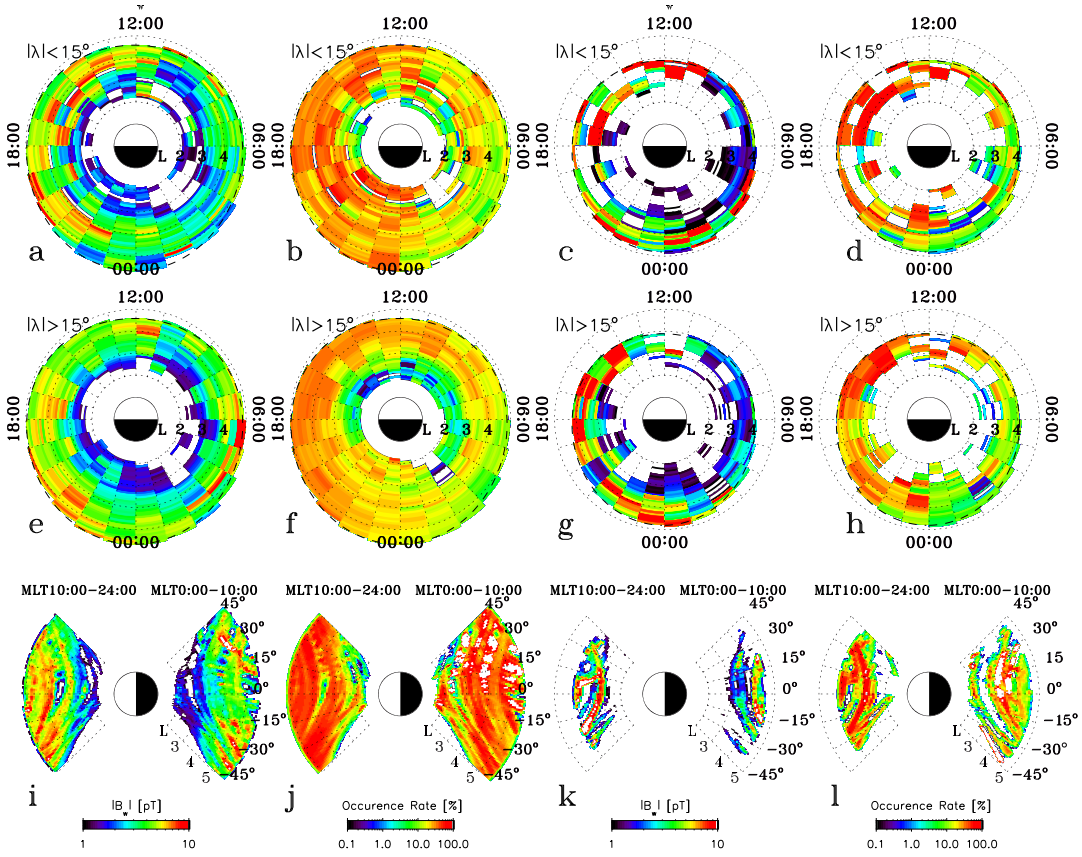
Figure 5. The averaged wave magnetic field intensity and occurrence rate of plasmaspheric hiss in the same format as in Figure 3.

and presented the statistics with more details. Obtained plasmaspheric hiss intensity and occurrence rate distributions are consistent with previous studies based on measurements aboard the DE-1 [*André et al.*, 2002]. Spatial distribution is close to obtained from CRRES data by *Meredith et al.* [2004].

3.2. Statistical Characteristics of ELF/VLF Wave Normal Directions in the Inner Magnetosphere

[21] Chorus waves are usually assumed to be generated in the close vicinity of the magnetic equator [*Lauben et al.*, 2002; *Parrot et al.*, 2003; *Santolík et al.*, 2004, 2005]. Here we examine this assumption by studying the direction of the Poynting vector. The prevalent direction of wave propagation along the background magnetic field $\vec{B}_0$ is given by the normalized parameter $P = (N_a - N_o)/(N_a + N_o)$, where N_a and

N_o are the number of spectra having a Poynting flux directed along ($\vec{k} \cdot \vec{B}_0 > 0$) and opposite ($\vec{k} \cdot \vec{B}_0 < 0$) to $\vec{B}_0$, respectively. P varies in the range from –1 to 1. A value of P near 0 corresponds to an equal number of wave events with propagation direction along and opposite to the background magnetic field. P distribution for the chorus outside the plasmasphere (L =4–7) where chorus generated at the equator dominate is shown in Figure 6. Chorus show a sharp boundary at the equator (thickness about $1°$–$2°$) with a jump of P from about –0.6 to 0.6 (Figures 6a and 6b). A more chaotic behavior is observed in the night sector for high geomagnetic activity (Figure 6b). For plasmaspheric hiss waves, the behavior of P is more chaotic: P is close to 0 for all λ [*Agapitov et al.*, 2012].

[22] The PDFs of θ for the plasmaspheric hiss in the day and the night sectors of the magnetosphere are shown in Figures 7a and 7b for $K_p \leq 3$ and $K_p > 3$, respectively.
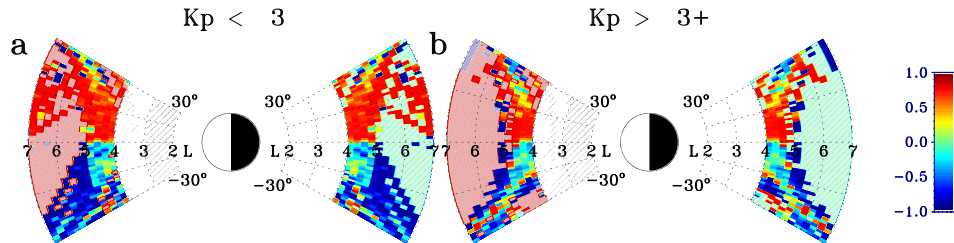

Figure 6. The dominant direction of the Poynting flux for chorus. Two geomagnetic activity regimes are shown: (a) low ($K_p \leq 3$) and (b) high ($K_p > 3$).
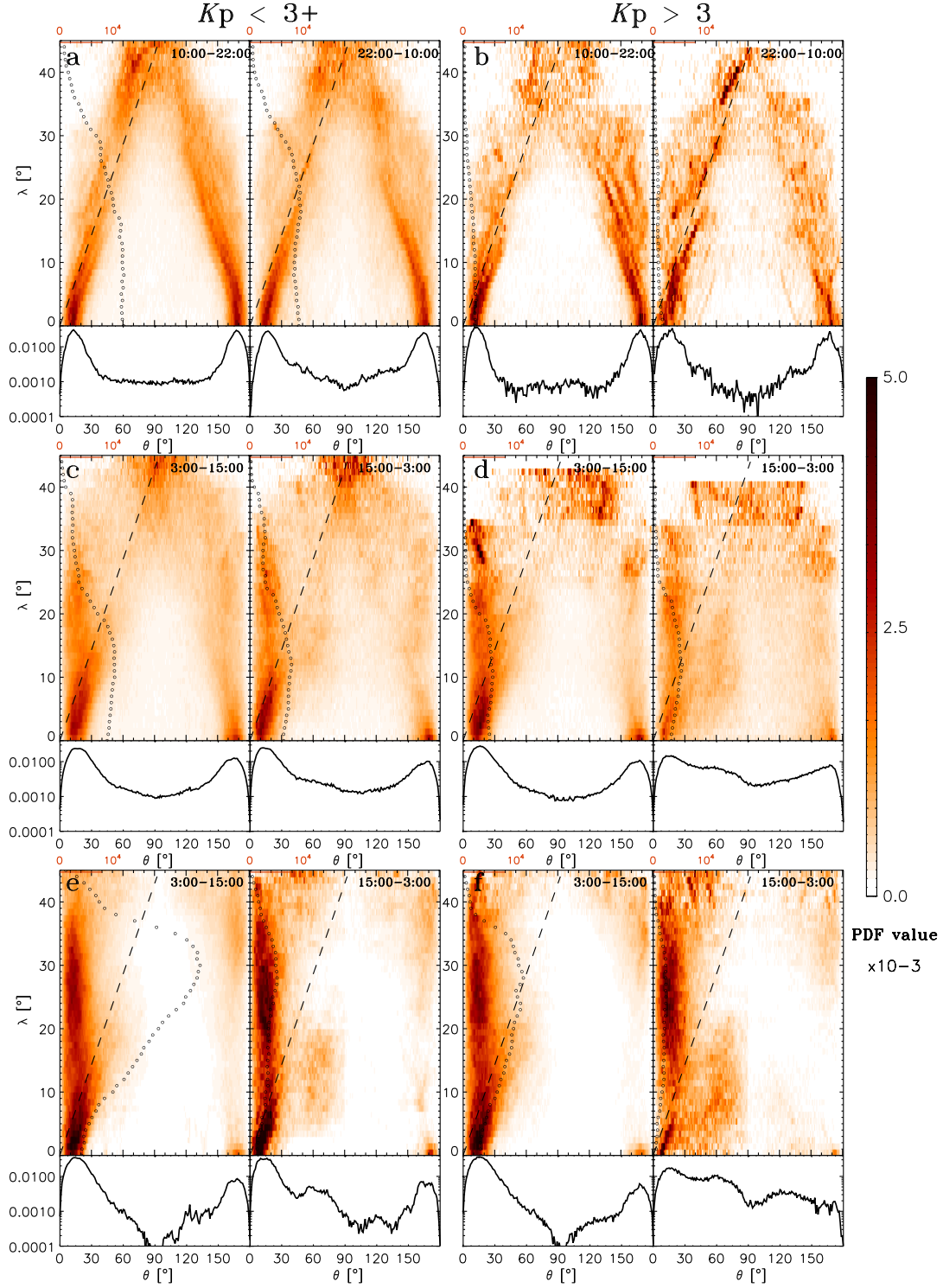
Figure 7. Distribution of θ for different λ. Figure 7a show θ distribution of the plasmaspheric hiss for low geomagnetic activity. In the Figure 7a, day and night sector distributions of θ are presented in the left and the right panels, respectively. Bottom panels in Figure 7a show the equatorial ($|\lambda| < 5°$) distributions of θ for plasmaspheric hiss. The approximation of θ dependence on λ presented in section 4 is shown by black dashed line. Number of measurements for each λ is indicated by black circles with the scale in the top. Figure 7b shows distributions of plasmaspheric hiss θ for high geomagnetic activity in the same format. In the Figures 7c and 7d distributions of θ for chorus waves ($4 < L < 5.5$) are presented in the same format for $K_p \leq 3$ and $K_p > 3$, respectively. Figures 7e and 7f show the distributions of θ for chorus in the L-shell range from 5.5 to 10.
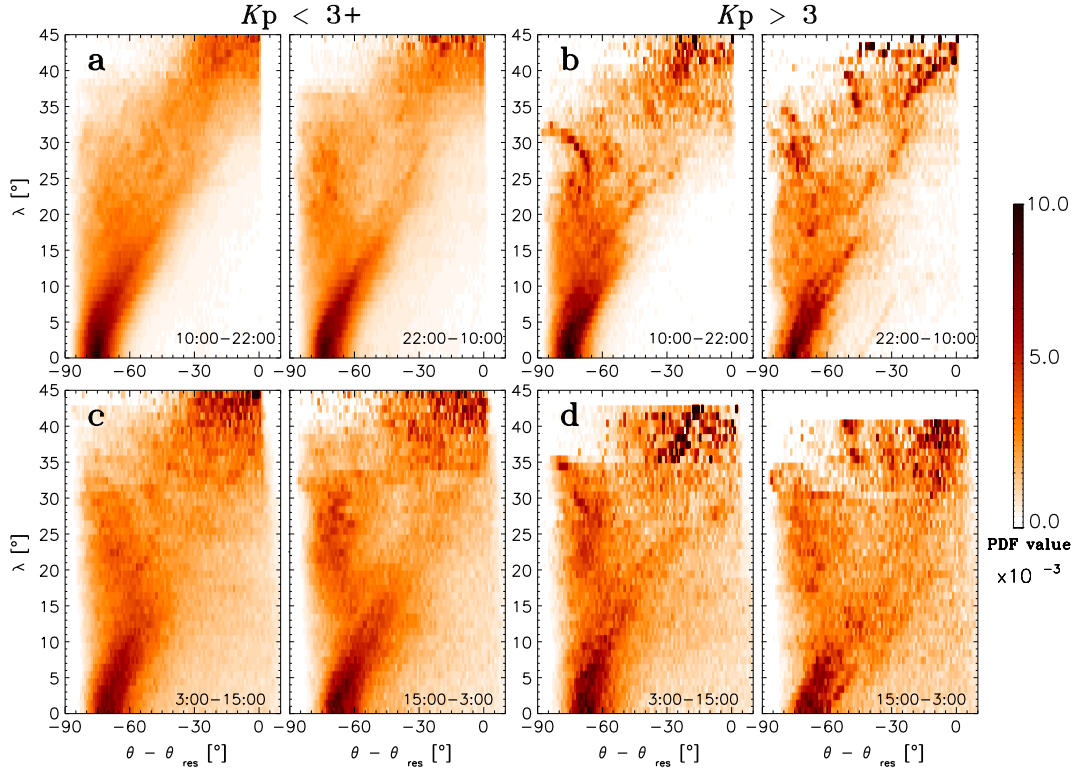
Figure 8. Difference between θ—the angle between the wave vector and the background magnetic field—and θ_{res}. An approximate value was used $\theta_{res} \approx \arccos(f/f_{ce})$ ($4 < L < 5.5$) for (a and b) chorus and (c and d) hiss frequency ranges. Magnetospheric sectors and geomagnetic activity levels are the same as in Figure 7.

Generally, the distributions are close to parallel at the equator with an increase of the mean value and of the variance of the θ-distribution with $|\lambda|$. The plasmaspheric hiss wave normal properties are consistent with numerical ray-tracing results for plasmaspheric hiss presented by *Bortnik et al.* [2011]. There, wave normals are quasi-parallel in the vicinity of the equator, but they deviate rapidly from the direction of the background magnetic field with increasing λ, later reaching the resonance cone. Waves can be reflected near $\lambda \geq 30°$ where the wave frequency becomes less than the local f_{LH}. The total number of wave events with propagation direction to and from the equator for the hiss are rather equivalent. During high geomagnetic activity periods in the night sector, quasi-parallel hiss waves are observed up to $\lambda \sim 25°$ together with oblique waves.

[23] The PDFs of the LB chorus θ as a function of λ are shown in Figure 7 (c and d) for $L < 5.5$ and (e and f) for $5.5 < L < 10$. In the first range of L-shells, both the mean value and the variance of the θ distribution increase with $|\lambda|$. A growth of θ with $|\lambda|$ is observed (wave normals approaching the resonance cone at $\lambda \approx 25°$, which is well reproduced by numerical ray-tracing simulations) [*Breuillard et al.*, 2012]. However, the number of detected oblique waves (as well as their amplitude) decreases rapidly. Simultaneously, quasi-parallel waves ($\theta \approx 10°–30°$) are observed, and this group becomes dominant for $|\lambda|$ between $10°$ and $30°$. The quasi-parallel population of LB chorus at middle latitudes is more significant in the night sector (Figure 7c) and during high geomagnetic activity (Figure 7d). These results are consistent with the wave normal angle distribution obtained

from POLAR measurements by *Haque et al.* [2010]. The probability of finding waves with $\theta > 20°$ decreases for $|\lambda| > 25°$, possibly because waves with high wave normal angles are more affected by Landau damping at higher $|\lambda|$ [*Burton and Holzer*, 1974; *Bortnik et al.*, 2011, 2006]. LB chorus wave normals tend to become transverse again only at $|\lambda| > 40°$, where the wave frequency becomes less than the local f_{LH} and reflection can occur. It is worth noting that the decrease of the wave magnetic component at $|\lambda| > 35°$ (Figure 4) is caused by the transformation of the electromagnetic mode into a quasi-electrostatic one. A significant amount of wave power resides in oblique waves for $L = 3.5$ to 5.5 at $|\lambda| > 10°$, as well as for $L = 5.5–10$ at $|\lambda| \sim 5°–20°$. Therefore, the main physical implications for oblique waves drawn in our previous papers [*Artemyev et al.*, 2012a, 2012b; *Mourenas et al.*, 2012a, 2012b] should remain roughly appropriate, at least for $L < 5.5$. The equatorial distribution of θ has a maximum at $\theta = 11°$ in the day sector and at $\theta = 13°$ in the night sector (quite close to THEMIS observations presented by *Li et al.* [2011]). The θ-values are generally smaller in the day sector than in the night sector, but in the night sector, θ values have a wider distribution. Mainly, the quasi-parallel chorus wave propagation is observed for $L > 5.5$ at all λ. A secondary maximum at $|\theta| = 60°$ in the outer magnetosphere can be seen in Figures 7e and 7f (at $\sim 70°$ from THEMIS data) [*Li et al.*, 2011].

[24] The observed properties of θ distribution partially can be explained by effects of wave Landau damping along the raypath: attenuation of oblique waves and possible amplification of quasi-parallel waves. The rate of
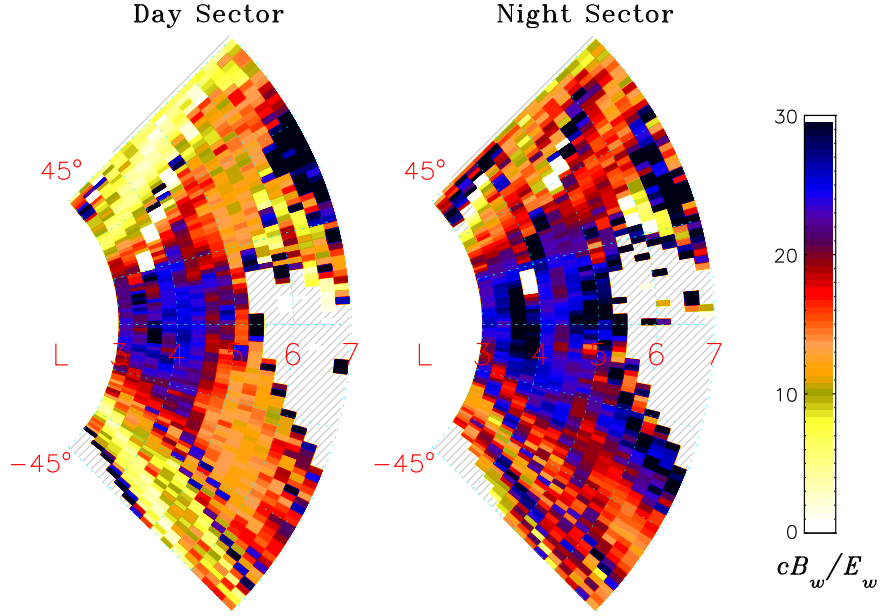
Figure 9. The ratio $c|B_w|/|E_w|$ in $\lambda - L$-shell frame. The median values of $c|B_w|/|E_w|$ PDF (the channel with the central frequency equal to 1760 Hz) are shown for (left) day and (right) night sectors.

Landau damping, based on an empirical nonthermal electron model grows with wave normal angles [*Chen et al.*, 2012], increases at larger L-shell, is larger on nightside than on dayside, and increases during more active geomagnetic condition that is well consistent with the observed behavior of θ distribution.

4. Discussion

[25] Several important aspects of our analysis should be taken into account in order to understand the characteristic features of the observed PDFs. Our analysis was performed in the fixed frequency range of the STAFF-SA instrument (8 Hz–4 kHz). Waves at higher λ (with higher magnitudes of $|\vec{B}_0|$) have a smaller range of ratios (f/f_{ce}), which corresponds to a potentially larger deviation of the wave normals from the magnetic field direction. On the other hand, waves detected at a particular location at higher λ are generated at different L-shells at the equator, resulting in a larger angular width of the distribution. The same peculiarities are obtained for plasmaspheric hiss waves (Figures 7a and 7b), but the propagation direction is more chaotic. The distribution of θ is rather symmetric near the equator. Similar results were obtained numerically by *Bortnik et al.* [2011] and by *Breuillard et al.* [2012] using a ray-tracing technique. It was shown that at high λ, the wave normals are predominantly oblique, but near the equator, the wave normal distribution can be either predominantly field aligned (at lower L-shells), or bimodal, having a maximum in the field-aligned direction and another maximum at very oblique angles.

[26] Figure 8 shows the difference $\theta - \theta_{res}$ for the chorus (for $L<5.5$) and plasmaspheric hiss. At higher λ, the background magnetic field magnitude increases along the wave raypath. As wave frequencies become closer to the local f_{LH}, wave normals deviate toward the perpendicular direction, and, finally, the wave normals approach the resonance cone and become nearly perpendicular to $\vec{B}_0$ for wave frequencies below the local f_{LH}. As the wave normal becomes more oblique, the component of the wave vector along $\vec{B}_0$ becomes smaller, and both the parallel and the perpendicular components of the wave group velocity decrease [*Shklyar et al.*, 2004]. Therefore, waves propagate slower at higher λ and spend more time in high-latitude regions, giving rise to a peak in amplitude of the statistical distribution at $\theta \sim 90°$ (Figure 4). The same effect results in similar properties for the distributions of the reflected waves propagating toward the equator. At higher λ, both the poleward and equatorward propagating waves shift toward perpendicular angles, and the energy flux of the reflected waves becomes comparable with the one of the direct waves. The two peaks of the distribution approach one another, and the frequency becomes close to f_{LH} for hiss waves. At $|\lambda| \approx 30°$, the two peaks merge, forming a common distribution with a peak spread of approximately $\theta \sim 90°$ and having an angular width of the same order. For chorus waves, the behavior of the θ-distribution at the higher λ can be explained by mixing of the chorus wave coming from wide range of L-shells.

[27] The direct evaluation of the θ distribution can be also checked from the ratio $c|B_w|/|E_w|$. This ratio depends on f_{pe}/f_{ce}, f/f_{ce}, and θ and varies in a wide range in the Earth's magnetosphere (mainly > 20 for wave normals directed along the background magnetic field). The value of $c|B_w|/|E_w|$ is greater than 10 for all values of f_{pe}/f_{ce} and f/f_{ce}, but this value decreases very fast for θ close to θ_{res} (if $c|B_w|/|E_w|$ less than 1, then $\theta \simeq \theta_{res}$). The ratio $c|B_w|/|E_w|$ can be estimated by use of STAFF-SA power spectral density measurements of three magnetic field and two electric field components. The median values of the $c|B_w|/|E_w|$ PDF (the channel with the central frequency equal to 1760 Hz) are shown in Figure 9 for day and night sectors. The observed decrease of $c|B_w|/|E_w|$ with λ is close to the dependence of the most probable value of θ, shown by *Agapitov et al.* [2011b].

[28] To estimate the deflection of the wave normal angle from the local background magnetic field direction in the vicinity of the equator, we use the simplified dispersion relation $\omega = \Omega_c k_\parallel k c^2 (k^2 c^2 + \omega_{pe}^2)^{-1}$, where $\omega = 2\pi f$, $\omega_{pe} = 2\pi f_{pe}$, and $\Omega_c = 2\pi f_{ce}$ [*Helliwell*, 1965]. The plasma density is assumed to be constant along field lines [see *Sheeley et al.*, 2001]. If the initial (equatorial) value of the wave normal angle $\theta = \sqrt{k^2 - k_\parallel^2}/k_\parallel$ is small, then we can use the approximation $k \approx k_\parallel$. In this case, we have two equations of ray tracing: $\partial k_\parallel/\partial t = \partial\omega/\partial s$ and $\partial s/\partial t = -\partial\omega/\partial k_\parallel$, where s is the parallel coordinate along the field line and $\Omega_c = \Omega_c(s)$ [*Breuillard et al.*, 2012]. The solution of these two equations is $k_\parallel \sqrt{\Omega_c - \omega} = $ const, and for $\Omega_c \gg \omega$, we have $k_\parallel \sqrt{\Omega_c} = $ const. Therefore, if at the equator, we have $\theta \approx 0$, then θ changes accordingly to the expression $\theta = \arccos\sqrt{\Omega_{0c}/\Omega_c}$, where $\Omega_{0c} = \Omega_c$ at $\lambda = 0$. Using the dipole magnetic field model $\sqrt{\Omega_{0c}/\Omega_c} = \cos^3\lambda/(1 + 3\sin^2\lambda)^{1/4}$ for small λ ($\sqrt{\Omega_{0c}/\Omega_c} \approx 1 - (9/4)\lambda^2$ and $\cos\theta \approx 1 - (1/2)\theta^2$), a simplified expression can be obtained $\theta \approx 2.1|\lambda|$, i.e., already at $|\lambda| \sim 10^\circ$, the deviation of the wave normal from the magnetic field should be around 20°. The coefficient of proportionality $\theta \approx 2.1|\lambda|$ is close to the observed value for the plasmaspheric hiss and for the chorus. Here we should mention that approximation $\theta \approx 2.1|\lambda|$ can be used up to $|\lambda| \sim 30^\circ$, where deviation from the expression $\theta = \arccos\sqrt{\Omega_{c0}/\Omega_c}$ reaches 10%. This approximation is shown in Figure 7 by dashed line and corresponds well with plasmaspheric hiss θ distribution. In the plasmasphere, Landau damping is low, and waves propagate without sufficient damping.

[29] Ray tracing explains successfully the behavior of whistler waves in the plasmasphere [*Bortnik et al.*, 2011] where plasma is cold and nonthermal particle fluxes are rare. Outside the plasmasphere (especially at $L > 5$), conversely, Landau damping could control the wave normal distribution properties [*Chen et al.*, 2012]: Oblique waves have a maximal attenuation (the maximum occurs at $\theta \simeq 50^\circ$–70°) [*Ginzburg and Rukhadze*, 1975], but quasi-parallel waves($|\theta| < 30^\circ$) propagate without significant damping. Thus, waves with intermediate wave normal angles pointing toward the Earth at the equator are generally less affected by Landau damping and able to propagate to higher latitude than other directions and contribute to field-aligned wave population at $5^\circ < \lambda < 15^\circ$. The LB chorus amplitude distribution as a function of λ presented by *Artemyev et al.* [2012b] and *Horne et al.* [2005] peaks at $\lambda \approx 15^\circ$–20°. At these λ, the emissions come predominately from the equatorial source at the same L-shell [*Breuillard et al.*, 2012]; thus, some wave amplification (mostly effective for parallel waves) may affect wave propagation up to $\lambda \approx 10^\circ$–15°.

5. Conclusions

[30] The global distribution of the whistler wave amplitudes and wave normal angles has been studied using STAFF-SA data from Cluster for lower band chorus and hiss waves separately. We present the distributions of wave intensity and wave normal angles based on the statistical study of wave measurements obtained from the Cluster 4 satellite from 2001 to 2010. The statistical database spans the radiation belts region, L-shells from 2 to 10, over a wide range of latitudes for quiet and active geomagnetic conditions. The most intense equatorial chorus waves are observed in the range from 4:00 to 14:00 MLT (10:00–15:00 MLT for mid-latitude chorus) and for L-shells from 7 to 10; plasmaspheric hiss waves are mainly seen from 11:00 to 22:00 MLT and for L-shells from 3 to 5, (this maximum was already shown by *André et al.* [2002] using the DE-1 data set). The statistical characteristics of the distributions are different for low ($K_p \leq 3$) and high ($K_p > 3$) geomagnetic activity. Two distinguishable regions exist where the wave amplitudes and the wave normal distributions exhibit different statistical properties under the low and high geomagnetic activity, as follows: (1) for $L = 2 - 4$ (up to the plasmapause) where lightning-generated and plasmaspheric hiss whistlers dominate; and (2) in a region where chorus-type whistlers dominate, for $L = 4 - 7$. Our study extends the ELF/VLF wave statistics for L-shells from 3 to 7 for the existing databases based on DE-1, CRRES, Cluster, and THEMIS measurements. The obtained spatial distributions are consistent with the earlier plasmaspheric hiss observations aboard DE-1 [*André et al.*, 2002; *Green et al.*, 2005] and aboard CRRES [*Meredith et al.*, 2004], and lower band chorus statistics from CRRES [*Meredith et al.*, 2001], THEMIS [*Cully et al.*, 2008; *Li et al.*, 2009; *Meredith et al.*, 2004, 2012], and Cluster [*Pokhotelov et al.*, 2008; *Meredith et al.*, 2012]. The wave magnetic and electric field amplitude distribution on the dayside has a minimum near the equator. As latitude increases up to 15°–25°, the wave amplitude increases to maximum values of the wave magnetic field up to 90 pT during low geomagnetic activity periods and up to 200 pT for high geomagnetic activity. The night sector wave amplitude distribution has a peak of about 100 pT near the equator ($-15^\circ < \lambda < 15^\circ$) during high geomagnetic activity periods. Amplitude maximum is observed on the equator also for $K_p < 3$ at $L > 6$; for $L < 6$, amplitude distribution is close to the day sector distribution (with equatorial amplitude minimum) but with lower amplitudes. These results therefore confirm the results obtained by *Horne et al.* [2005] on the basis of CRRES measurements for high geomagnetic activity intervals.

[31] We have obtained the statistical distribution of the wave normal directions as a function of λ and L-shell. The distribution of θ at the geomagnetic equator was concentrated in a 30° cone, with a maximum around 10°–15°. Due to curvature of the background magnetic field lines and the magnetic field magnitude gradient, wave normals tend to rotate outward the Earth increasing the mean value and the variance of the θ distribution along the raypath. The probability density functions of the wave amplitudes and wave normals are usually nonsymmetric and have significant non-Gaussian tails. The plasmaspheric hiss showed the most clear dependence of θ on λ for all wave amplitudes: θ mean value increases and roughly equal to 2.1λ for $|\lambda| > 10^\circ$, reaching the resonance angle at $|\lambda| \sim 30^\circ$–40°. Small group of field-aligned waves was observed at $10^\circ < \lambda < 30^\circ$ mainly in the nightside and during more active geomagnetic conditions. The plasmaspheric hiss propagated both directions from the equator and to the equator with rather similar amplitudes. The obtained distributions are well consistent with numerical results presented by *Bortnik et al.* [2011] and our analytical estimate. Chorus propagated away from the equatorial source region starting from θ mean values about 15°. Here, our results are similar to previous results based on measurements in the vicinity of the equator presented by

Burton and Holzer [1974], *Hayakawa et al.* [1984], *Agapitov et al.* [2010], *Li et al.* [2011], and *Agapitov et al.* [2011a]. As λ increases, the θ-distribution spreads toward more oblique angles also increasing the variance of the θ distribution which is consistent with the results obtained by *Burton and Holzer* [1974], *Muto et al.* [1987], and *Haque et al.* [2010] for lower band chorus waves and by *Hayakawa et al.* [1986] for hiss waves and well reproduced by numerical ray-tracing simulations [*Breuillard et al.*, 2012]. Then, wave normals approach the resonance cone, waves propagate in a quasi-electrostatic mode till their reflection at $|\lambda| \sim 25°$–$40°$ that is seen in the growth of wave electric field amplitudes $|\lambda| > 20°$–$30°$. A rapid decrease of the probability to find very oblique chorus waves with $\theta > 60°$ at $\lambda > 25°$–$40°$ is observed (similar results were obtained from POLAR measurements [*Haque et al.*, 2010]); thus, field-aligned waves become dominate at $20° < |\lambda| < 35°$. The decreasing of the oblique lower band chorus population is observed with increase of L-shell. The quasi parallel wave population is much more significant with increasing of the L-shell, in the night sector (Figure 7) and during high geomagnetic activity, which presumably can be explained by the effects of Landau dumping [*Chen et al.*, 2012]. Thus, wave attenuation and amplification have to be taken into account to obtain a correct model of wave distribution out of the plasmasphere.

[32] These results have important implications for the modeling of the diffusion processes due to wave-particle resonant interactions. The ELF/VLF wave polarization properties obtained here can sufficiently change the resonance conditions for wave-particle interactions. Conventional averaging procedures should not be performed without taking into account the relatively rapid deviation of wave normals from the quasi-parallel direction of propagation. Calculations of pitch angle diffusion coefficients which account for the oblique propagation of the whistler waves and the dependence of θ distribution on λ, show that electron pitch angle and energy diffusion is significantly increased for electrons with small pitch angles [*Artemyev et al.*, 2012a; *Mourenas et al.*, 2012b; *Artemyev et al.*, 2013] in comparison with the approximation of parallel wave propagation [*Glauert and Horne*, 2005], due to the contribution of the higher-order cyclotron resonances. It is worth noting that obtained results of distribution of normal angles can play an important role for models of nonlinear wave-particle interaction [*Shklyar and Matsumoto*, 2009]. Presence of the finite population of very oblique whistler waves leads to new perspective of particle acceleration by trapping into Landau resonance [e.g., *Artemyev et al.*, 2012c, and references therein]. Therefore, the wave intensity and wave normal distributions obtained here should be taken into account for future studies of electron resonant scattering and acceleration.

References

Agapitov, O., V. Krasnoselskikh, Y. Zaliznyak, V. Angelopoulos, O. Le Contel, and G. Rolland (2010), Chorus source region localization in the Earth's outer magnetosphere using THEMIS measurements, *Ann. Geophys.*, 28, 1377–1386.

Agapitov, O., V. Krasnoselskikh, T. Dudok de Wit, Y. Khotyaintsev, J. S. Pickett, O. Santolík, and G. Rolland (2011a), Multispacecraft observations of chorus emissions as a tool for the plasma density fluctuations' remote sensing, *J. Geophys. Res.*, 116, A09222, doi:10.1029/2011JA016540.

Agapitov, O., V. Krasnoselskikh, Y. V. Khotyaintsev, and G. Rolland (2011b), A statistical study of the propagation characteristics of whistler waves observed by Cluster, *Geophys. Res. Lett.*, 38, L20103, doi:10.1029/2011GL049597.

Agapitov, O., V. Krasnoselskikh, Y. V. Khotyaintsev, and G. Rolland (2012), Correction to "A statistical study of the propagation characteristics of whistler waves observed by Cluster", *Geophys. Res. Lett.*, 39, L24102, doi:10.1029/2012GL054320.

Agapitov, O., V. Krasnoselskikh, Y. Zaliznyak, V. Angelopoulos, O. Le Contel, and G. Rolland (2011c), Observations and modeling of forward and reflected chorus waves captured by THEMIS, *Ann. Geophys.*, 29, 541–550, doi:10.5194/angeo-29-541-2011.

André, R., F. Lefeuvre, F. Simonet, and U. S. Inan (2002), A first approach to model the low-frequency wave activity in the plasmasphere, *Ann. Geophys.*, 20, 981–996, doi:10.5194/angeo-20-981-2002.

Artemyev, A., O. Agapitov, H. Breuillard, V. Krasnoselskikh, and G. Rolland (2012a), Electron pitch-angle diffusion in radiation belts: The effects of whistler wave oblique propagation, *Geophys. Res. Lett.*, 39, L08105, doi:10.1029/2012GL051393.

Artemyev, A., O. Agapitov, V. Krasnoselskikh, H. Breuillard, and G. Rolland (2012b), Statistical model of electron pitch-angle diffusion in the outer radiation belt, *J. Geophys. Res.*, 117, A08219, doi:10.1029/2012JA017826.

Artemyev, A. V., V. V. Krasnoselskikh, O. V. Agapitov, D. Mourenas, and G. Rolland (2012c), Non-diffusive resonant acceleration of electrons in the radiation belts, *Phys. Plasmas*, 19, 122901, doi:10.1063/1.4769726.

Artemyev, A. V., D. Mourenas, O. V. Agapitov, and V. V. Krasnoselskikh (2013), Parametric validations of analytical lifetime estimates for radiation belt electron diffusion by whistler waves, *Ann. Geophys.*, 31, 599–624, doi:10.5194/angeo-31-599-2013.

Balogh, A., et al. (2001), The Cluster magnetic field investigation: Overview of in-flight performance and initial results, *Ann. Geophys.*, 19, 1207–1217, doi:10.5194/angeo-19-1207-2001.

Bortnik, J., U. S. Inan, and T. F. Bell (2006), Landau damping and resultant unidirectional propagation of chorus waves, *Geophys. Res. Lett.*, 33, L03102, doi:10.1029/2005GL024553.

Bortnik, J., L. Chen, W. Li, R. M. Thorne, N. P. Meredith, and R. B. Horne (2011), Modeling the wave power distribution and characteristics of plasmaspheric hiss, *J. Geophys. Res.*, 116, A12209, doi:10.1029/2011JA016862.

Breuillard, H., Y. Zaliznyak, V. Krasnoselskikh, O. Agapitov, A. Artemyev, and G. Rolland (2012), Chorus wave-normal statistics in the Earth's radiation belts from ray tracing technique, *Ann. Geophys.*, 30, 1223–1233.

Bunch, N. L., M. Spasojevic, and Y. Y. Shprits (2012), Off-equatorial chorus occurrence and wave amplitude distributions as observed by the Polar Plasma Wave Instrument, *J. Geophys. Res.*, 117, A04205, doi:10.1029/2011JA017228.

Burton, R. K., and R. E. Holzer (1974), The origin and propagation of chorus in the outer magnetosphere, *J. Geophys. Res.*, 79, 1014–1023, doi:10.1029/JA079i007p01014.

Chen, L., J. Bortnik, W. Li, and R. M. Thorne (2012), Modeling the wave power distribution and characteristics of plasmaspheric hiss, *J. Geophys. Res.*, 116(A12), doi:10.1029/2011JA016862.

Chum, J., O. Santolik, D. A. Gurnett, and J. S. Pickett (2009), Oblique lower band chorus waves: Time shifts between discrete elements observed by the Cluster spacecraft, *J. Geophys. Res.*, 114, A00F02, doi:10.1029/2009JA014366.

Cornilleau-Wehrlin, N., et al. (1997), The cluster spatio-temporal analysis of field fluctuations (staff) experiment, *Space Sci. Rev.*, 79, 107–136, doi:10.1023/A:1004979209565.

Cornilleau-Wehrlin, N., et al. (2003), First results obtained by the Cluster STAFF experiment, *Ann. Geophys.*, *21*, 437–456, doi:10.5194/angeo-21-437-2003.

Cully, C. M., J. W. Bonnell, and R. E. Ergun (2008), THEMIS observations of long-lived regions of large-amplitude whistler waves in the inner magnetosphere, *Geophys. Res. Lett.*, *35*, L17S16, doi:10.1029/2008GL033643.

Doe, R. A., M. B. Moldwin, and M. Mendillo (1992), Plasmapause morphology determined from an empirical ionospheric convection model, *J. Geophys. Res.*, *97*, A00F02, doi:10.1029/91JA01649.

Ginzburg, V. L., and A. A. Rukhadze (1975), *Waves in Magnetoactive Plasma*, 256 pp., Izdatel'stvo Nauka, Moscow, Russia. http://adsabs.harvard.edu/abs/1975MoIzN....S....G.

Glauert, S. A., and R. B. Horne (2005), Calculation of pitch angle and energy diffusion coefficients with the PADIE code, *J. Geophys. Res.*, *110*, A04206, doi:10.1029/2004JA010851.

Goldstein, B. E., and B. T. Tsurutani (1984), Wave normal directions of chorus near the equatorial source region, *J. Geophys. Res.*, *89*, 2789–2810, doi:10.1029/JA089iA05p02789.

Green, J. L., S. Boardsen, L. Garcia, W. W. L. Taylor, S. F. Fung, and B. W. Reinisch (2005), On the origin of whistler mode radiation in the plasmasphere, *J. Geophys. Res.*, *110*, A03201, doi:10.1029/2004JA010495.

Gustafsson, G., et al. (2001), First results of electric field and density observations by Cluster EFW based on initial months of operation, *Ann. Geophys.*, *19*, 1219–1240, doi:10.5194/angeo-19-1219-2001.

Haque, N., M. Spasojevic, O. Santolík, and U. S. Inan (2010), Wave normal angles of magnetospheric chorus emissions observed on the Polar spacecraft, *J. Geophys. Res.*, *115*, A00F07, doi:10.1029/2009JA014717.

Hayakawa, M., Y. Yamanaka, M. Parrot, and F. Lefeuvre (1984), The wave normals of magnetospheric chorus emissions observed on board GEOS 2, *J. Geophys. Res.*, *89*, 2811–2821, doi:10.1029/JA089iA05p02811.

Hayakawa, M., N. Ohmi, M. Parrot, and F. Lefeuvre (1986), Direction finding of ELF hiss emissions in a detached plasma region of the magnetosphere, *J. Geophys. Res.*, *91*, 135–141.

Helliwell, R. A. (1965), *Whistlers and Related Ionospheric Phenomena*, 343 pp., Stanford University Press, USA.

Horne, R. B., R. M. Thorne, S. A. Glauert, J. M. Albert, N. P. Meredith, and R. R. Anderson (2005), Timescale for radiation belt electron acceleration by whistler mode chorus waves, *J. Geophys. Res.*, *110*, A03225, doi:10.1029/2004JA010811.

Kennel, C. F., and H. E. Petschek (1966), Limit on stably trapped particle fluxes, *J. Geophys. Res.*, *71*(1), 1–28, doi:10.1029/JZ071i001p00001.

King, J. H., and N. E. Papitashvili (2005), Solar wind spatial scales in and comparisons of hourly Wind and ACE plasma and magnetic field data, *J. Geophys. Res.*, *110*, A02104, doi:10.1029/2004JA010649.

Khotyaintsev, Y., P.-A. Lindqvist, A. Eriksson, and M. André (2010), *The EFW Data in the CAA*, in The Cluster Active Archive, *Studying the Earth's Space Plasma Environment*, edited by H. Laakso, M. G. T. T. Taylor, and C. P. Escoubet, pp. 97–108. Astrophysics and Space Science Proceedings, Berlin, Springer.

Lauben, D. S., U. S. Inan, T. F. Bell, and D. A. Gurnett (2002), Source characteristics of ELF/VLF chorus, *J. Geophys. Res.*, *107*, 1429, doi:10.1029/2000JA003019.

Li, W., J. Bortnik, R. M. Thorne, and V. Angelopoulos (2011), Global distribution of wave amplitudes and wave normal angles of chorus waves using THEMIS wave observations, *J. Geophys. Res.*, *116*, A12205, doi:10.1029/2011JA017035.

Li, W., et al. (2009), Global distribution of whistler-mode chorus waves observed on the THEMIS spacecraft, *Geophys. Res. Lett.*, *36*, L09104, doi:10.1029/2009GL037595.

Lyons, L. R. (1974a), General relations for resonant particle diffusion in pitch angle and energy, *J. Plasma Phys.*, *12*, 45, doi:10.1017/S0022377800024910.

Lyons, L. R. (1974b), Pitch angle and energy diffusion coefficients from resonant interactions with ion-cyclotron and whistler waves, *J. Plasma Phys.*, *12*, 417–432, doi:10.1017/S002237780002537X.

Lyons, L. R., and R. M. Thorne (1973), Equilibrium structure of radiation belt electrons, *J. Geophys. Res.*, *78*, 2142–2149, doi:10.1029/JA078i013p02142.

Means, J. D. (1972), Use of the three-dimensional covariance matrix in analyzing the polarization properties of plane waves, *J. Geophys. Res.*, *77*, 5551–5559, doi:10.1029/JA077i028p05551.

Meredith, N. P., R. B. Horne, and R. R. Anderson (2001), Substorm dependence of chorus amplitudes: Implications for the acceleration of electrons to relativistic energies, *J. Geophys. Res.*, *106*, 13,165–13,178, doi:10.1029/2000JA900156.

Meredith, N. P., R. B. Horne, R. M. Thorne, D. Summers, and R. R. Anderson (2004), Substorm dependence of plasmaspheric hiss, *J. Geophys. Res.*, *109*, A06209, doi:10.1029/2004JA010387.

Meredith, N. P., R. B. Horne, M. A. Clilverd, D. Horsfall, R. M. Thorne, and R. R. Anderson (2006), Origin of plasmaspheric hiss, *J. Geophys. Res.*, *111*, A09217, doi:10.1029/2006JA011707.

Meredith, N. P., R. B. Horne, A. Sicard-Piet, D. Boscher, K. H. Yearby, W. Li, and R. M. Thorne (2012), Global model of lower band and upper band chorus from multiple satellite observations, *J. Geophys. Res.*, *117*, A10225, doi:10.1029/2012JA017978.

Mourenas, D., A. V. Artemyev, J.-F. Ripoll, O. V. Agapitov, and V. V. Krasnoselskikh (2012a), Timescales for electron quasi-linear diffusion by parallel and oblique lower-band Chorus waves, *J. Geophys. Res.*, *117*, A06234, doi:10.1029/2012JA017717.

Mourenas, D., A. V. Artemyev, O. V. Agapitov, and V. V. Krasnoselskikh (2012b), Acceleration of radiation belts electrons by very oblique chorus waves, *J. Geophys. Res.*, *117*, A10212, doi:10.1029/2012JA018041.

Muto, H., M. Hayakawa, M. Parrot, and F. Lefeuvre (1987), Direction finding of half-gyrofrequency VLF emissions in the off-equatorial region of the magnetosphere and their generation and propagation, *J. Geophys. Res.*, *92*, 7538–7550, doi:10.1029/JA092iA07p07538.

Ni, B., R. M. Thorne, N. P. Meredith, Y. Y. Shprits, and R. B. Horne (2011), Diffuse auroral scattering by whistler mode chorus waves: Dependence on wave normal angle distribution, *J. Geophys. Res.*, *116*, A10207, doi:10.1029/2011JA016517.

Parrot, M., O. Santolýk, N. Cornilleau-Wehrlin, M. Maksimovic, and C. C. Harvey (2003), Source location of chorus emissions observed by Cluster, *Ann. Geophys.*, *21*, 473–480, doi:10.5194/angeo-21-473-2003.

Pokhotelov, D., F. Lefeuvre, R. B. Horne, and N. Cornilleau-Wehrlin (2008), Survey of ELF-VLF plasma waves in outer radiation belt observed by Cluster STAFF-SA experiment, *Ann. Geophys.*, *26*, 3269–3277, doi:10.5194/angeo-26-3269-2008.

Santolík, O., D. A. Gurnett, J. S. Pickett, J. Chum, and N. Cornilleau-Wehrlin (2009), Oblique propagation of whistler mode waves in the chorus source region, *J. Geophys. Res.*, *114*, A00F03, doi:10.1029/2009JA014586.

Santolík, O., D. A. Gurnett, and J. S. Pickett (2004), Multipoint investigation of the source region of storm-time chorus, *Ann. Geophys.*, *22*, 2555–2563.

Santolík, O., D. A. Gurnett, J. S. Pickett, M. Parrot, and N. Cornilleau-Wehrlin (2005), Central position of the source region of storm-time chorus, *Planet. Space Sci.*, *53*, 299–305.

Sheeley, B. W., M. B. Moldwin, H. K. Rassoul, and R. R. Anderson (2001), An empirical plasmasphere and trough density model: CRRES observations, *J. Geophys. Res.*, *106*, 25,631–25,642, doi:10.1029/2000JA000286.

Shklyar, D., J. Chum, and F. Jirícek (2004), Characteristic properties of Nu whistlers as inferred from observations and numerical modelling, *Ann. Geophys.*, *22*, 3589–3606, doi:10.5194/angeo-22-3589-2004.

Shklyar, D., and H. Matsumoto (2009), Oblique whistler-mode waves in the inhomogeneous magnetospheric plasma: Resonant interactions with energetic charged particles, *Surv. Geophys.*, *30*, 55–104, doi:10.1007/s10712-009-9061-7.

Shprits, Y. Y., and B. Ni (2009), Dependence of the quasi-linear scattering rates on the wave normal distribution of chorus waves, *J. Geophys. Res.*, *114*, A11205, doi:10.1029/2009JA014223.

Stix, T. H. (1962), The theory of plasma waves, in *Waves in Plasmas*, 566 pp., Springer.

Summers, D., B. Ni, and N. P. Meredith (2007), Timescales for radiation belt electron acceleration and loss due to resonant wave-particle interactions: 1. Theory, *J. Geophys. Res.*, *112*, A04206, doi:10.1029/2006JA011801.

Thorne, R. M., E. J. Smith, R. K. Burton, and R. E. Holzer (1973), Plasmaspheric hiss, *J. Geophys. Res.*, *78*, 1581–1596, doi:10.1029/JA078i010p01581.

Tsurutani, B., and E. Smith (1977), Two types of magnetospheric ELF chorus and their substorm dependences, *J. Geophys. Res.*, *82*(A32), 5112–5128, doi:10.1029/0JGREA000082000A32005112000001.